Applied Physics Letters

RESEARCH ARTICLE | NOVEMBER 24 2025

Superinductor-based ultrastrong coupling in a superconducting circuit

Alba Torras-Coloma ; Luca Cozzolino ; Ariadna Gómez-del-Pulgar-Martínez ; Elia Bertoldo ; P. Forn-Díaz

Check for updates

Appl. Phys. Lett. 127, 214002 (2025)
https://doi.org/10.1063/5.0293790

View Online
Export Citation

Articles You May Be Interested In

Implementation of scalable suspended superinductors

Appl. Phys. Lett. (January 2025)

Operating in a deep underground facility improves the locking of gradiometric fluxonium qubits at the sweet spots

Appl. Phys. Lett. (February 2022)

Three-Josephson junctions flux qubit couplings

Appl. Phys. Lett. (December 2021)

16 December 2025 12:49:54

BLUE FORS

More wiring. More qubits. More results.
The world's most popular fridge just got better.

Discover the new side-loading LD system

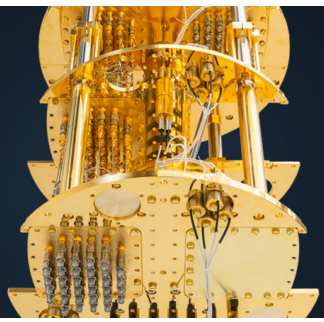

AIP Publishing

Applied Physics Letters ARTICLE pubs.aip.org/aip/apl

Superinductor-based ultrastrong coupling in a superconducting circuit

Cite as: Appl. Phys. Lett. **127**, 214002 (2025); doi: 10.1063/5.0293790
Submitted: 30 July 2025 · Accepted: 2 November 2025 ·
Published Online: 24 November 2025

View Online Export Citation CrossMark

Alba Torras-Coloma,[1,2,a] Luca Cozzolino,[1,2,b] Ariadna Gómez-del-Pulgar-Martínez,[2,3,4] Elia Bertoldo,[2] and P. Forn-Díaz[2,5,a]

AFFILIATIONS

[1]Departament de Física, Universitat Autònoma de Barcelona, 08193 Bellaterra, Spain
[2]Institut de Física d'Altes Energies (IFAE), The Barcelona Institute of Science and Technology (BIST), Bellaterra (Barcelona) 08193, Spain
[3]Barcelona Supercomputing Center, Barcelona 08034, Spain
[4]Departament de Física Quàntica i Astrofísica, Universitat de Barcelona, Barcelona 08028, Spain
[5]Qilimanjaro Quantum Tech SL, Barcelona, Spain

[a]**Authors to whom correspondence should be addressed:** Alba.Torras@autonoma.cat and pforndiaz@ifae.es
[b]**Present address:** Qilimanjaro Quantum Tech. SL, Barcelona, Spain.

ABSTRACT

We present an ultrastrong superinductor-based coupling mechanism in a circuit consisting of a flux qubit galvanically coupled to an LC resonator. The coupling inductor is fabricated with granular aluminum, a superinductor material able to provide large surface inductances. Despite the low persistent current exhibited by the qubit, $I_p = 11.6\,\mathrm{nA}$, spectroscopy measurements reveal a Bloch–Siegert shift of 23 MHz and a coupling fraction of $g/\omega_r \simeq 0.13$, entering the perturbative ultrastrong coupling regime. An independent estimate of the coupler inductance by low-temperature resistance measurements leads to $L_c = (0.74 \pm 0.14)\,\mathrm{nH}$, which is compatible with $g/\omega_r \gtrsim 0.1$. Our results show that superinductors are a promising resource to study ultrastrong coupling physics in high-coherence circuits using flux qubits with small loop areas and low persistent currents.

© 2025 Author(s). All article content, except where otherwise noted, is licensed under a Creative Commons Attribution-NonCommercial 4.0 International (CC BY-NC) license (https://creativecommons.org/licenses/by-nc/4.0/). https://doi.org/10.1063/5.0293790

16 December 2025 12:49:54

Understanding the interaction between light and matter in superconducting quantum circuits[1,2] has been key to developing applications in areas such as quantum computing[3] and quantum sensing.[4] One advantage of superconducting circuits with respect to, e.g., atomic systems is the tunability of device parameters to achieve a light–matter coupling strength g in a wide range of values. Previous experiments in qubit-resonator circuits[5–7] attained coupling strengths that represent a significant fraction of the excitation frequencies, entering the so-called ultrastrong coupling (USC) regime.[8,9] This boundary is defined by interaction strengths in the range $g/\omega_r \gtrsim 0.1$, where ω_r is the bare frequency of the resonator.[10] Beyond this boundary, the system cannot be considered as two independent bodies, leading to new physics with potential applications in quantum information science.[11,12]

Different methods exist to achieve ultrastrong couplings in superconducting quantum circuits. Inductive ultrastrong couplings between flux qubits and resonators have typically been achieved using a shared Josephson junction.[5,7,13–15] However, Josephson junction couplings have a main disadvantage of introducing stray nonlinearities in the circuit that can influence the resonator mode, in addition to possible losses from two-level defects[16] and quasiparticles.[17] In contrast, superinductors provide a large inductance while exhibiting a low level of nonlinearities and low dissipation,[18] resulting in a promising alternative to Josephson junctions as couplers for coherent USC studies. So far, superinductors have been realized by three different approaches: Josephson junction arrays,[18–22] geometric inductors,[23,24] and disordered superconductors.[25] Disordered superconductors, such as those based on nitrides[26–29] or oxides,[25,30,31] naturally display a large sheet kinetic inductance, which in some cases can go up to several nH per unit area. This property can be exploited in flux-like qubits to design relatively small structures exhibiting a large and significantly linear inductance,[32] which is favorable for coherent dynamics given that $1/f$ flux noise scales with both the device size[33] as well as the qubit persistent current, $T_1^{-1}, T_\varphi^{-1} \propto I_p^2$.[34–37] Despite potential decoherence channels such as quasiparticles, two-level system defects, and $1/f$ noise in disordered superconductors like granular aluminum (grAl), qubits fabricated entirely from grAl have shown coherence

© Author(s) 2025

times compatible with those of high-coherence junction-based flux qubits.[25,38]

In this work, we present a superinductor-based coupling in a qubit-resonator circuit where the coupling is large enough to reach the USC regime. The device used consists of a three-junction flux qubit galvanically coupled to a lumped-element LC resonator. The coupling inductor is made of grAl,[25,39,40] leading to smaller qubit loops and lower persistent currents compared to those of flux qubits used in previous USC experiments. The use of a superinductor material is a key design feature to reach couplings in the USC regime without compromising qubit coherence times.

The circuit schematic used in this work is presented in Fig. 1(a). The qubit loop is interrupted by three Josephson junctions of energy E_J and capacitance C_J, one of which is smaller by a factor α. By means of a shared inductance L_c, the qubit is galvanically coupled to an LC oscillator of inductance L_R and capacitance C_R. As shown in Sec. A of the supplementary material, this system can be described by the so-called quantum Rabi Hamiltonian,[41]

$$\hat{\mathscr{H}}_{\mathrm{QRM}} = \hbar\frac{\Omega_q}{2}\hat{\sigma}_z + \hbar\omega_r\left(\hat{a}^\dagger\hat{a} + \frac{1}{2}\right) + \hbar g\hat{\sigma}_x(\hat{a} + \hat{a}^\dagger), \quad (1)$$

where $\hat{\sigma}_i$ are the Pauli operators, g is the coupling strength, and ω_r and Ω_q are the resonator and qubit frequencies, respectively. Equation (1) can be rewritten in the flux qubit persistent current basis,

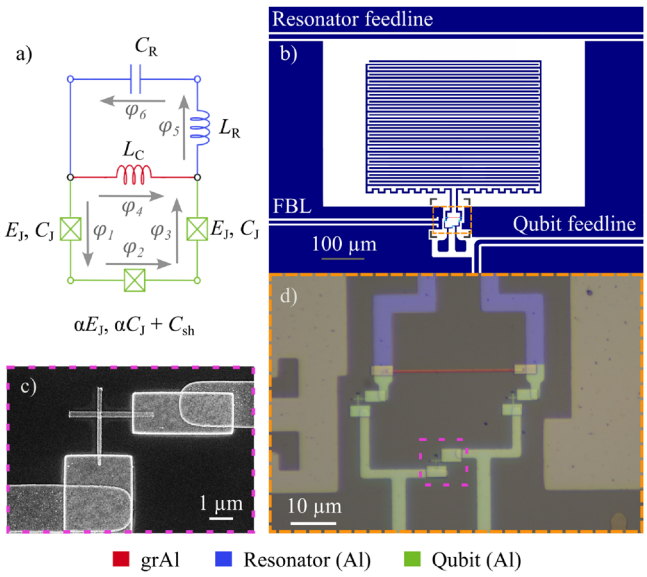

FIG. 1. Qubit-resonator circuit layout. (a) Circuit schematics used to derive the full system Hamiltonian. The central junction of the qubit loop is smaller by a factor α. The qubit and the resonator are coupled by sharing an inductor L_c. (b) Design layout of the system consisting of a lumped-element resonator galvanically coupled to a three-junction flux qubit. The device contains two feedlines to selectively drive through the resonator or the qubit. (c) Scanning electron micrograph (SEM) image of the small qubit Josephson junction. (d) False-colored optical microscope image of the device. The colors indicate the materials used in each part of the chip. The grAl inductor, the qubit, and the resonator are shown in red, green, and blue, respectively. The dark gray area corresponds to the Si substrate while the Al ground plane is highlighted in a lighter gray.

$$\hat{\mathscr{H}}_{\mathrm{QRM}} = -\frac{1}{2}(\epsilon\hat{\sigma}_z + \Delta\hat{\sigma}_x) + \hbar\omega_r\left(\hat{a}^\dagger\hat{a} + \frac{1}{2}\right) + \hbar g\hat{\sigma}_z(\hat{a} + \hat{a}^\dagger), \quad (2)$$

where Δ is the qubit energy gap, and $\epsilon = 2I_p(\Phi_{ext} - \Phi_0/2)$ is the magnetic energy of the qubit with I_p the persistent current and Φ_{ext} the external magnetic flux.

In galvanically coupled qubit-resonator circuits such as the one in Fig. 1(a), an additional oscillator mode exists, which is mainly determined from the combination of the coupling inductor L_c and the qubit capacitances. In the perturbative USC regime, the frequency of this extra oscillator mode is at a much higher frequency than the qubit and can be adiabatically eliminated. Under this approximation, the qubit-resonator coupling strength can be estimated using[42]

$$g \simeq \xi_R\frac{L_{\mathrm{eff}}I_pI_{\mathrm{rms,R}}}{\hbar} = \xi_R\frac{L_{\mathrm{eff}}I_p}{\hbar Z_R}\sqrt{\frac{\hbar\omega_R}{2C_R}}, \quad (3)$$

where $L_{\mathrm{eff}}^{-1} \equiv L_R^{-1} + L_c^{-1}$ is an effective inductance, $\omega_R \equiv (C_RL_R)^{-1/2}$ is the bare resonator frequency and ξ_R is a coefficient that approaches 1 in our circuit.[43] $I_{\mathrm{rms,R}} = (\hbar\omega_R/2L_R)^{1/2}$ and $Z_R = (L_R/C_R)^{1/2}$ are the root-mean squared current and the impedance of the bare resonator, respectively. Note that, due to the coupling inductor L_c, the resonator frequency in Eq. (1) can be approximated as $\omega_r \simeq [(L_R + L_c)C_R]^{-1/2}$, which differs from the bare resonator frequency ω_R (see Sec. A of the supplementary material).

In Fig. 1(b), we present the design layout of the device. Two feedlines capacitively couple to the resonator (top line) and to the shunt capacitor C_{sh} of the qubit (bottom line), allowing the extraction of information from this hybrid system through different observables.[44] The circuit also contains a flux line coupling to the qubit loop. The lumped-element resonator is designed with a large capacitance to decrease its impedance, maximizing Eq. (3). The capacitance and inductance of the resonator are designed with values $C_R = 0.74$ pH and $L_R = 0.9$ nH. The qubit consists of three Josephson junctions, where the central one is a factor $\alpha = 0.58$ smaller.

The device is fabricated in five lithography steps on an intrinsic Si substrate. The ground plane, feedlines, and resonator are fabricated using optical lithography and are evaporated with 50 nm of Al. The grAl, Josephson junctions, and contacts are fabricated consecutively in independent electron-beam lithography steps. We adjust the resistance of grAl, and thus its kinetic inductance L_k, by both the oxygen flow used in the evaporation process and by the width of the coupling trace.[39] In Table I, we provide a list of values obtained for grAl evaporated at 0.2 nm/s and different oxygen flows. For the present device,

TABLE I. GrAl calibration for 50 nm thick samples evaporated at 0.2 nm/s. R_s is the resistance measured at room-temperature as a function of the oxygen flow during the evaporation and R_s' is the resistance after a 13 min bake at 200° C.

O_2 flow (sccm)	R_s ($\Omega/\square$)	R_s' ($\Omega/\square$)
0.0	0.89 ± 0.06	0.89 ± 0.05
0.2	2.96 ± 0.20	2.75 ± 0.19
0.4	7.56 ± 2.97	5.01 ± 0.77
0.6	17.31 ± 2.48	14.57 ± 1.49
0.8	43.49 ± 25.09	35.14 ± 19.96

16 December 2025 12:49:54

© Author(s) 2025

we use a flow of 0.6 sccm for an expected sheet kinetic inductance of ∼10 pH/□. The detailed process of fabrication is described in Sec. E of the supplementary material. Images of the resulting device are shown in Figs. 1(c) and 1(d). The false-colored regions indicate the different parts of the circuit.

We estimate the resistivity, ρ, and L_k of the coupler from its dimensions and resistance at room temperature and at 4 K. The grAl coupler is $(30.0\pm0.9)\,\mu$m long and (487 ± 15) nm wide. The room-temperature resistance of the wire is extracted by measuring one of the test structures, giving $R_{RT} = (0.96\pm0.01)\,$kΩ. Using the length of the coupler and the thickness of the film, (50 ± 5) nm, we extract the room-temperature resistivity of the grAl line, $\rho_{RT} = (78.3\pm8.5)\,\mu\Omega$ cm. In order to estimate the grAl inductance, we perform resistance measurements as a function of temperature on one of the grAl structures. We obtain a normal resistance at 4 K of $R_{4K} = (0.86\pm0.01)\,$kΩ and a critical temperature of $T_c = (1.60\pm0.31)$ K (see Sec. F of the supplementary material). Using the Mattis–Bardeen formula for complex conductivity in the local, dirty limit at low frequency ($hf \ll k_B T$) and in the low-temperature limit ($T \ll T_c$),[40]

$$L_k = 0.18\frac{\hbar R_{4K}}{k_B T_c}, \tag{4}$$

we estimate the kinetic inductance of the grAl coupler to be $L_c = (0.74\pm0.14)$ nH. The estimated frequency and impedance of the resonator considering the renormalization effect of L_c is $\omega_r/2\pi \simeq 4.569$ GHz and $Z'_R \equiv [(L_R + L_c)/C_R]^{1/2} \simeq 47.1\,\Omega$. The qubit gap Δ is designed close to ω_r by taking into account the renormalization effect of the coupling inductor L_c on the qubit properties (see Sec. B of the supplementary material for more details). Using Eq. (3), we estimate the coupling to be $g/2\pi \simeq 0.67$ GHz for a qubit with $I_p \simeq 19.6$ nA. The low I_p value of the qubit is one of the key design features and is obtained by fabricating Josephson junctions with an extracted critical current density of $J_c = (0.66\pm0.03)\,\mu\text{A}/\mu\text{m}^2$ (see Sec. B of the supplementary material).

The sample is mounted on the baseplate of a dilution refrigerator with a base temperature of 20 mK. We measure the transmission spectrum of the system independently through the qubit (S_{21}^{Q}) or through the resonator (S_{21}^{R}) feedlines. An external coil is used to tune the qubit flux Φ_{ext}. In Fig. 2, we compare single-tone transmission measurements $S_{21}^{Q,R}$ vs Φ_{ext}. The magnitude of the transmission for each frequency value f_i is normalized as $\{|S_{21}(f_i,\Phi_{ext})| - \min(|S_{21}|(f_i,\Phi_{ext}))\}/\text{std}(|S_{21}|(f_i,\Phi_{ext}))$. The normalization is used to mask the spurious box modes present in the signal (see Sec. D of the supplementary material). In both measurements, one can identify a high-frequency transition ω_{02} exhibiting usual flux qubit spectral features, an intermediate frequency ω_{01} mostly insensitive to flux except around $\Phi_{ext} = \Phi_0/2$, and a third transition ω_{12}, which is much weaker and extends toward lower frequencies.

We observe minor differences between the spectra shown in Figs. 2(a) and 2(b). All transitions are well defined in both plots $|S_{21}^{Q,R}|$, with a difference of ∼5 dB outside the sweet spot when probing the system through the resonator (see the raw data provided in Sec. D of the supplementary material). These observations are in contrast to the expected system response,[44] where qubit (resonator) driving excites qubit (resonator)-like observables. This should translate into a visible qubit (resonator)-like transition $\omega_{02}(\omega_{01})$ at (away from) the sweet spot in Figs. 2(a) and 2(b) only for direct qubit (resonator) driving. We

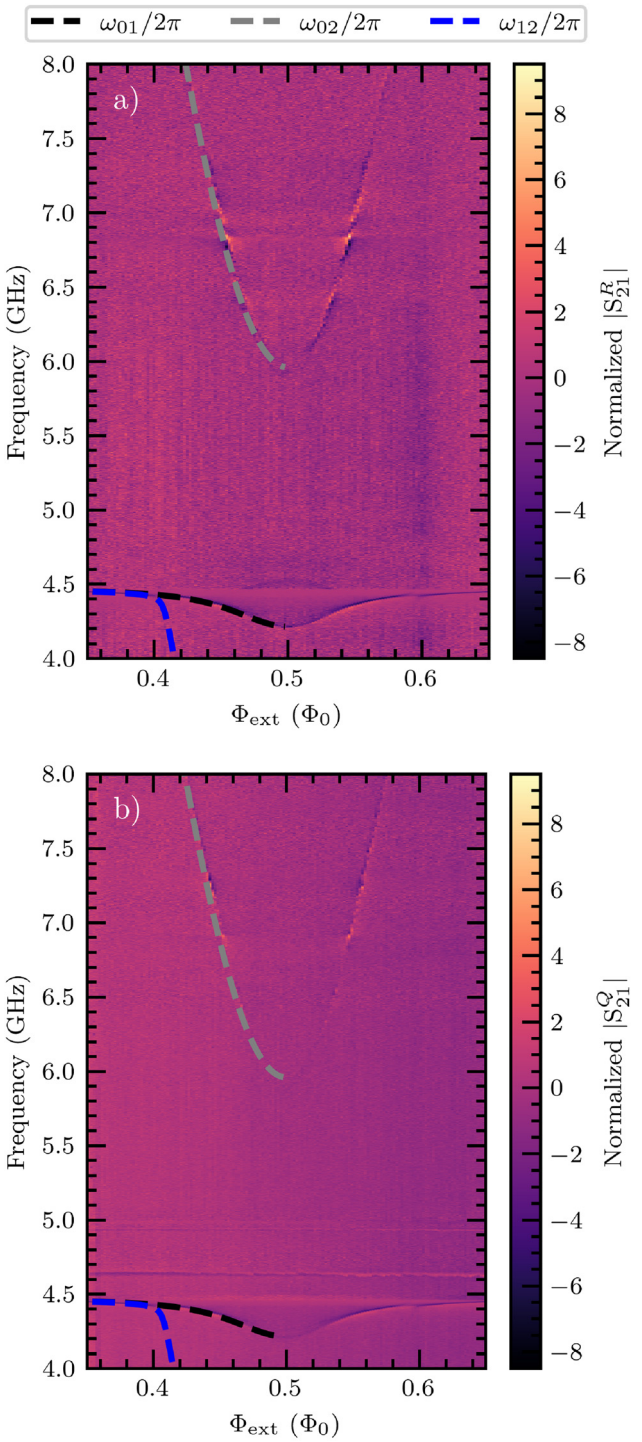

FIG. 2. Normalized transmission magnitude $|S_{21}|$ vs flux bias (Φ_{ext}) obtained via single-tone spectroscopy. The expression used for the signal normalization is given in the main text. The dashed lines correspond to the fitted quantum Rabi model [Eq. (1)] with fitting parameters ω_r, Δ, I_p, and g. (a) Spectrum obtained through measuring the resonator feedline, $|S_{21}^R|$. (b) Spectrum obtained through measuring the qubit feedline, $|S_{21}^Q|$.

16 December 2025 12:49:54

© Author(s) 2025

believe that the discrepancy between theory and experiment on the device studied originates from a stray inductive coupling of the resonator to the qubit feedline (see Sec. C of the supplementary material).

In Fig. 3, we show the normalized transmission of the two-tone spectroscopy vs flux using the values of $\omega_{01}(\Phi_{ext})$ as probe. We identify four different transitions in the spectrum. ω_{01} is mostly resonator-like and is the one used for the two-tone spectroscopy measurement. ω_{02} is also present in the single-tone spectra and is mostly qubit-like. We also identify more clearly the intermediate transition ω_{12} corresponding to the exchange of an excitation between qubit and resonator. Outside the sweet spot, we identify a two-photon qubit-like transition $\omega_{03}/2$. An additional transition is visible between 4.5 and 5.5 GHz, which seems to match to a type of three-photon blue-sideband transition $\hbar(\omega_{03}+\omega_{01})/3$.

Using the observed single-tone and two-tone transitions, the spectrum can be fitted to Eq. (2). The resulting parameters of the fit are $I_p = (11.619 \pm 0.004)$ nA, $\Delta/h = (5.707 \pm 0.002)$ GHz, $\omega_r/2\pi = (4.463 \pm 0.001)$ GHz, and $g/2\pi = (0.578 \pm 0.001)$ GHz. The fitted resonator frequency is compatible with the frequency $\omega_r/2\pi = 4.465$ GHz obtained as the saturation of $\omega_{01}(\Phi_{ext})$ at high powers, similar to a punch-out measurement,[45] and just 104 MHz lower than our estimate. The coupling achieved is consistent with our estimate of L_k with Eq. (3). Despite the small value of I_p, the fraction $g/\omega_r \simeq 0.13 > 0.1$ still falls in the perturbative USC regime. Increasing the coupler superinductance further can bring the coupling easily to $g/\omega_r > 0.3$ while still keeping low persistent currents and relatively small qubit loops, which is advantageous to attain long coherence times.

The fitted parameters can be used to calculate the spectrum using the Jaynes–Cummings (JC) Hamiltonian.[46] The difference between the QRM and the JC curves in the perturbative USC regime is the Bloch–Siegert shift, ω_{BS}, an effect of the counter-rotating terms.[6] ω_{BS} is maximum at the sweet spot with a value of 23 MHz for the ω_{01} transition (see Sec. D1 of the supplementary material for more details). The qubit-like transition (ω_{02}) suffers the same shift but in the opposite direction. The observation of the Bloch–Siegert shift is conclusive proof that the circuit studied in this work is described by the physics of the USC regime, despite the low I_p, and validates our approach to further advance the investigation of applications of USC physics for quantum science and technology.

In conclusion, we have presented a superinductor-based coupling consisting of a shared grAl wire between a flux qubit and a resonator. We show that although the persistent current of the qubit is low compared to previous USC experiments, the superinductor has enough contribution to bring the system into the USC regime ($g/\omega_r > 0.1$) while keeping qubit loop dimensions below $10^3\ \mu m^2$. We validate our

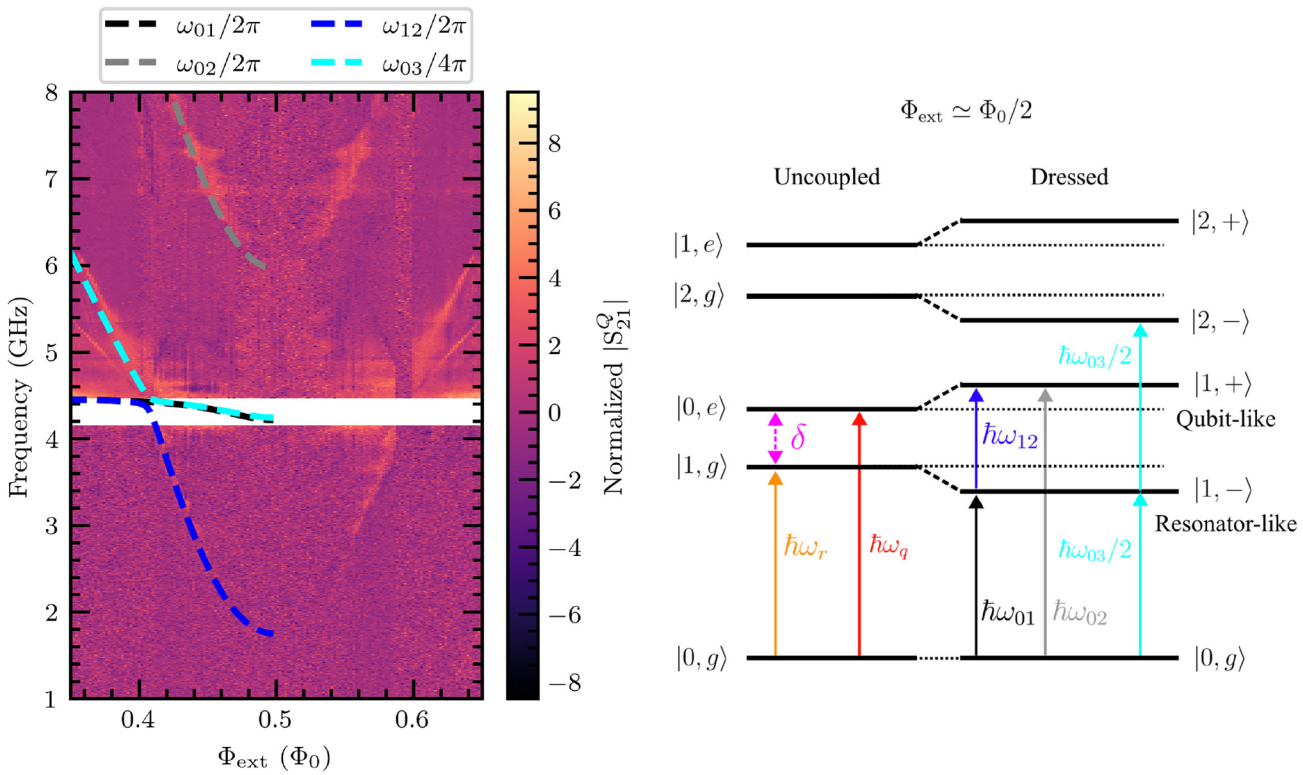

FIG. 3. Spectrum and energy ladder of the system. Left panel: Normalized transmission magnitude vs flux bias (Φ_{ext}) obtained via two-tone spectroscopy using the qubit feedline. The resonator tone is fixed at the frequencies defined by the ω_{01} transition measured using single-tone spectroscopy. The dashed lines correspond to the fitted quantum Rabi model spectrum with fit parameters ω_r, Δ, I_p, and g. In contrast to Fig. 2, we observe the two-photon transition $\omega_{03}/2$ and a second transition, which seems to match a three-photon sideband transition. Right panel: schematics of the uncoupled and dressed energy level transitions of the qubit-resonator system near the sweet spot. Given our specific circuit parameters, the single- and two-photon resonator-like transitions turn out to be very close in frequency.

16 December 2025 12:49:54

© Author(s) 2025

results by measuring and fitting the transmission spectra of our system to the quantum Rabi model. Owing to the large inductance provided by the superinductor, the design constraints to reach the ultrastrong coupling regime can be relaxed. This work opens the door to designing devices in the non-perturbative USC regime with low persistent current flux qubits and small qubit loops, thus leading to high-coherence times. Our sequential fabrication procedure also allows one to introduce other materials as couplers, such as nitride-based superconductors,[26,27] with potentially higher coherence times.

See the supplementary material for an overview of the theoretical circuit Hamiltonian derivation, crosstalk electromagnetic simulations, fabrication procedure, measured spectra, and granular aluminum critical temperature curve.

We would like to thank J. J. Garcia-Ripoll, L. Magazzù, and M. Grifoni for the fruitful discussions. We acknowledge funding from the Ministry of Economy and Competitiveness and Agencia Estatal de Investigacion (Nos. RYC2019-028482-I, PCI2019-111838-2, PID2021-122140NB-C31, and PCI2024-153468), the European Commission (FET-Open AVaQus GA 899561, QuantERA), and program "Doctorat Industrial" of the Agency for Management of University and Research Grants (2020 DI 41; 2024 DI 00004). IFAE is partially funded by the CERCA program of the Generalitat de Catalunya. This study was supported by MICIN with funding from European Union NextGenerationEU (No. PRTR-C17.I1) and by Generalitat de Catalunya. This work was (partially) supported by the Catalonia Quantum Academy, part of the Quantica-Mediterranean Valley of Quantum Science and Technologies initiative of the Generalitat of Catalunya.

AUTHOR DECLARATIONS

Conflict of Interest

The authors have no conflicts to disclose.

Author Contributions

Alba Torras-Coloma: Conceptualization (supporting); Data curation (lead); Formal analysis (lead); Investigation (equal); Methodology (equal); Software (lead); Visualization (equal); Writing – original draft (equal); Writing – review & editing (equal). **Luca Cozzolino:** Formal analysis (supporting); Investigation (supporting); Software (supporting); Writing – review & editing (supporting). **Ariadna Gómez-del-Pulgar-Martínez:** Investigation (supporting); Methodology (supporting); Writing – review & editing (supporting). **Elia Bertoldo:** Investigation (supporting); Methodology (supporting); Writing – review & editing (supporting). **Pol Forn-Diaz:** Conceptualization (lead); Data curation (supporting); Formal analysis (supporting); Funding acquisition (lead); Investigation (equal); Methodology (equal); Project administration (lead); Resources (lead); Supervision (lead); Validation (lead); Visualization (equal); Writing – original draft (equal); Writing – review & editing (equal).

DATA AVAILABILITY

The data that support the findings of this study are available from the corresponding authors upon reasonable request.

REFERENCES

[1]A. Blais, R.-S. Huang, A. Wallraff, S. M. Girvin, and R. J. Schoelkopf, Phys. Rev. A—At., Mol., Opt. Phys. **69**, 062320 (2004).
[2]A. Wallraff, D. I. Schuster, A. Blais, L. Frunzio, R.-S. Huang, J. Majer, S. Kumar, S. M. Girvin, and R. J. Schoelkopf, Nature **431**, 162 (2004).
[3]R. Stassi, M. Cirio, and F. Nori, npj Quantum Inf. **6**, 67 (2020).
[4]C. L. Degen, F. Reinhard, and P. Cappellaro, Rev. Mod. Phys. **89**, 035002 (2017).
[5]F. Yoshihara, T. Fuse, S. Ashhab, K. Kakuyanagi, S. Saito, and K. Semba, Nat. Phys. **13**, 44 (2017).
[6]P. Forn-Díaz, J. Lisenfeld, D. Marcos, J. J. Garcia-Ripoll, E. Solano, C. Harmans, and J. Mooij, Phys. Rev. Lett. **105**, 237001 (2010).
[7]T. Niemczyk, F. Deppe, H. Huebl, E. Menzel, F. Hocke, M. Schwarz, J. Garcia-Ripoll, D. Zueco, T. Hümmer, E. Solano *et al.*, Nat. Phys. **6**, 772 (2010).
[8]C. Ciuti, G. Bastard, and I. Carusotto, Phys. Rev. B—Condens. Matter Mater. Phys. **72**, 115303 (2005).
[9]J. Bourassa, J. M. Gambetta, A. A. Abdumalikov, Jr, O. Astafiev, Y. Nakamura, and A. Blais, Phys. Rev. A—At., Mol., Opt. Phys. **80**, 032109 (2009).
[10]D. Z. Rossatto, C. J. Villas-Bôas, M. Sanz, and E. Solano, Phys. Rev. A **96**, 013849 (2017).
[11]P. Forn-Díaz, L. Lamata, E. Rico, J. Kono, and E. Solano, Rev. Mod. Phys. **91**, 025005 (2019).
[12]A. Frisk Kockum, A. Miranowicz, S. De Liberato, S. Savasta, and F. Nori, Nat. Rev. Phys. **1**, 19 (2019).
[13]P. Forn-Diaz, J. J. García-Ripoll, B. Peropadre, J.-L. Orgiazzi, M. Yurtalan, R. Belyansky, C. M. Wilson, and A. Lupascu, Nat. Phys. **13**, 39 (2017).
[14]F. Yoshihara, T. Fuse, S. Ashhab, K. Kakuyanagi, S. Saito, and K. Semba, Phys. Rev. A **95**, 053824 (2017).
[15]A. Tomonaga, H. Mukai, F. Yoshihara, and J.-S. Tsai, Phys. Rev. B **104**, 224509 (2021).
[16]A. Bilmes, S. Zanker, A. Heimes, M. Marthaler, G. Schön, G. Weiss, A. V. Ustinov, and J. Lisenfeld, Phys. Rev. B **96**, 064504 (2017).
[17]D. Ristè, C. Bultink, M. J. Tiggelman, R. N. Schouten, K. W. Lehnert, and L. DiCarlo, Nat. Commun. **4**, 1913 (2013).
[18]V. Manucharyan, "Superinductance," Ph.D. thesis (Yale University, 2012).
[19]N. A. Masluk, I. M. Pop, A. Kamal, Z. K. Minev, and M. H. Devoret, Phys. Rev. Lett. **109**, 137002 (2012).
[20]M. Bell, I. Sadovskyy, L. Ioffe, A. Y. Kitaev, and M. Gershenson, Phys. Rev. Lett. **109**, 137003 (2012).
[21]V. E. Manucharyan, J. Koch, L. I. Glazman, and M. H. Devoret, Science **326**, 113 (2009).
[22]D. Fraudet, I. Snyman, D. M. Basko, S. Léger, T. Sépulcre, A. Ranadive, G. Le Gal, A. Torras-Coloma, W. Guichard, S. Florens *et al.*, Phys. Rev. Lett. **134**, 013804 (2025).
[23]M. Peruzzo, A. Trioni, F. Hassani, M. Zemlicka, and J. M. Fink, Phys. Rev. Appl. **14**, 044055 (2020).
[24]M. Peruzzo, F. Hassani, G. Szep, A. Trioni, E. Redchenko, M. Žemlička, and J. M. Fink, PRX Quantum **2**, 040341 (2021).
[25]L. Grünhaupt, M. Spiecker, D. Gusenkova, N. Maleeva, S. T. Skacel, I. Takmakov, F. Valenti, P. Winkel, H. Rotzinger, W. Wernsdorfer *et al.*, Nat. Mater. **18**, 816 (2019).
[26]D. Niepce, J. Burnett, and J. Bylander, Phys. Rev. Appl. **11**, 044014 (2019).
[27]A. Torras-Coloma, L. M. de Olcoz, E. Céspedes, E. Bertoldo, D. López-Núñez, S. Paul, W. Wernsdorfer, G. Rius, and P. Forn-Díaz, Supercond. Sci. Technol. **37**, 035017 (2024).
[28]H. G. Leduc, B. Bumble, P. K. Day, B. H. Eom, J. Gao, S. Golwala, B. A. Mazin, S. McHugh, A. Merrill, D. C. Moore *et al.*, Appl. Phys. Lett. **97**, 102509 (2010).
[29]M. R. Vissers, J. Gao, D. S. Wisbey, D. A. Hite, C. C. Tsuei, A. D. Corcoles, M. Steffen, and D. P. Pappas, Appl. Phys. Lett. **97**, 232509 (2010).
[30]P. Kamenov, W.-S. Lu, K. Kalashnikov, T. DiNapoli, M. T. Bell, and M. E. Gershenson, Phys. Rev. Appl. **13**, 054051 (2020).
[31]V. Gupta, P. Winkel, N. Thakur, P. van Vlaanderen, Y. Wang, S. Ganjam, L. Frunzio, and R. J. Schoelkopf, Phys. Rev. Appl. **23**, 054067 (2025).
[32]Josephson junction arrays and geometric superinductors can also be used to achieve large and linear inductors, however, they typically require larger

16 December 2025 12:49:54

© Author(s) 2025

structures which could impact the qubit loop dimensions thus enhancing their sensitivity to flux noise.
[33]J. Braumüller, L. Ding, A. P. Vepsäläinen, Y. Sung, M. Kjaergaard, T. Menke, R. Winik, D. Kim, B. M. Niedzielski, A. Melville *et al.*, Phys. Rev. Appl. **13**, 054079 (2020).
[34]F. Yoshihara, K. Harrabi, A. Niskanen, Y. Nakamura, and J. S. Tsai, Phys. Rev. Lett. **97**, 167001 (2006).
[35]C. H. van der Wal, F. Wilhelm, C. Harmans, and J. Mooij, Eur. Phys. J. B-Condens. Matter Complex Syst. **31**, 111 (2003).
[36]G. Ithier, E. Collin, P. Joyez, P. Meeson, D. Vion, D. Esteve, F. Chiarello, A. Shnirman, Y. Makhlin, J. Schriefl *et al.*, Phys. Rev. B—Condens. Matter Mater. Phys. **72**, 134519 (2005).
[37]A. Shnirman, Y. Makhlin, and G. Schön, Phys. Scr. **T102**, 147 (2002).
[38]D. Rieger, S. Günzler, M. Spiecker, P. Paluch, P. Winkel, L. Hahn, J. Hohmann, A. Bacher, W. Wernsdorfer, and I. Pop, Nat. Mater. **22**, 194 (2023).
[39]B. Abeles, R. W. Cohen, and G. Cullen, Phys. Rev. Lett. **17**, 632 (1966).
[40]H. Rotzinger, S. Skacel, M. Pfirrmann, J. Voss, J. Münzberg, S. Probst, P. Bushev, M. Weides, A. Ustinov, and J. Mooij, Supercond. Sci. Technol. **30**, 025002 (2017).
[41]I. Rabi, Phys. Rev. **49**, 324 (1936).
[42]A. Torras-Coloma, P. Forn-Díaz, and J. J. García-Ripoll, in preparation.
[43]The coefficient takes the form: $\xi_R^2 = \omega_R/\omega_A$ with $\omega_A^2 = \frac{\omega_R^2+\omega_4^2}{2} - \sqrt{\left(\frac{\Delta^2}{2}\right)^2 + \tilde{g}^4}$, $\omega_4^2 = 1/L_{\text{eff}}C_{\text{tot}}$, $\Delta^2 = \omega_R^2 - \omega_4^2$, $\tilde{g}^2 = \omega_R/\sqrt{L_R C_{\text{tot}}}$, and $C_{\text{tot}} = \alpha C_J + C_{\text{sh}}$. The details of the derivation will be provided in Ref. 42.
[44]L. Magazzù, P. Forn-Díaz, and M. Grifoni, Phys. Rev. A **104**, 053711 (2021).
[45]M. D. Reed, L. DiCarlo, B. Johnson, L. Sun, D. Schuster, L. Frunzio, and R. Schoelkopf, Phys. Rev. Lett. **105**, 173601 (2010).
[46]E. T. Jaynes and F. W. Cummings, Proc. IEEE **51**, 89 (1963).

16 December 2025 12:49:54

© Author(s) 2025